IEEE Open Journal of Vehicular Technology

Received 6 July 2023; accepted 30 August 2023. Date of publication 4 September 2023;
date of current version 22 September 2023. The review of this article was coordinated by Editor Beatriz Soret.

Digital Object Identifier 10.1109/OJVT.2023.3311544

Super-Large-Coverage Standardized Wireless Communication System and Its Implementation in VHF Band for IoT and V2X

KIMINOBU MAKINO [1,2] (Graduate Student Member, IEEE), KEIICHI MIZUTANI [1] (Member, IEEE), TAKESHI MATSUMURA [1] (Member, IEEE), AND HIROSHI HARADA [1] (Senior Member, IEEE)

[1]Graduate School of Informatics, Kyoto University, Kyoto 606-8501, Japan
[2]School of Platforms, Kyoto University, Kyoto 606-8501, Japan

CORRESPONDING AUTHOR: HIROSHI HARADA (e-mail: hiroshi.harada@i.kyoto-u.ac.jp)

This work was supported in part by the National Institute of Information and Communications Technology under Grant 05101 and in part by the ImPACT Program of Council for Science, Technology, and Innovation. An earlier version of this article was presented at the 20th International Symposium on Wireless Personal Multimedia Communications (WPMC), Yogyakarta, Dec. 2017 [doi: 10.1109/WPMC.2017.8301895].

ABSTRACT This article presents a comprehensive evaluation of the performance of a super-large-coverage mobile communication system for wireless regional area networks (WRANs) in the very-high-frequency (VHF) band. The system was standardized as ARIB STD-T103 and IEEE 802.16n. It can transmit data over a distance of 10 km or more at a transmission rate of several megabits per second (Mbps). It is particularly suitable for transmitting sensor and monitoring information, including moving images, over a wide area. First, we present some use cases and determine the feasibility of implementing WRANs for vehicle-to-everything (V2X) and the Internet of Things applications. Subsequently, we evaluate the transmission performance and estimate the transmission distance in the VHF-band radio propagation environment through computer simulations and experimental evaluations with our WRAN prototype. In the evaluation, we also adopt several channel estimation methods for a particular pilot pattern in the downlink. Moreover, we demonstrate the transmission distance that can be achieved with and without a multihop relay based on the evaluation results. Single-hop transmission reaches up to approximately 10 km while maintaining transmission speeds of several Mbps on the uplink, when QPSK is used. Conversely, by using multihop transmission, although the transmission speed is approximately 1/2 to 1/6, the maximum transmission distance is approximately 50 km.

INDEX TERMS Channel estimation, MRC diversity, OFDMA, VHF, WRAN.

I. INTRODUCTION

The implementation of cyber-physical system (CPS) platforms has significantly improved the Internet of Things (IoT) and vehicle-to-everything (V2X)-based applications in recent years [2]. CPSs transmit sensor, metering, and monitoring information from physical space to cyberspace. This information is processed in the cyberspace through machine learning, and the results are then fed back into the physical space to form value. A wide-area communication system is required to collect data from a wide area to configure a CPS platform for the IoT and V2X applications. The communication distance must be more than 10 km to implement the platform in various applications, such as intelligent transport systems (ITSs) with V2X, positioning, marine sensing, and ship-to-ship communication. Furthermore, a high mobility environment requires a transmission rate of at least several megabits per second (Mbps) since the information to be collected includes text and numerical data along with moving images. Table 1 lists the wireless communication systems that are currently available for V2X applications [1], [3], [4], [5], [6], [7].

Fourth-generation (4G) and fifth-generation mobile communication systems (5G), which are public communication systems standardized by the 3rd Generation Partnership Project (3GPP), can be considered for V2X communication

TABLE 1. Comparison Among Candidate Technologies for IoT and V2X Communications

	Traditional V2X		LPWA				Proposed
Technology	Cellular [3,6]	DSRC [3,7]	LoRa [3,5]	Sigfox [4,5]	NB-IoT [3,5]	eMTC [3]	WRAN [1]
Coverage	< 10 km	< 1.0 km	< 50 km	< 50 km	< 35 km	< 10 km	> 10 km
Data rate	20 Mbps	< 27 Mbps	250 kbps	100 bps	< 250 kbps	< 1 Mbps	< 8 Mbps
Mobility	Support	Support	Limited	Limited	Not support	Support	Support
Frequency band	UHF band	SHF band (5 GHz)	UHF band (Sub 1 GHz)	UHF band (Sub 1 GHz)	UHF band	UHF band	VHF band (200 MHz in Japan)
Band license	Licensed	Licensed	Unlicensed	Unlicensed	Licensed	Licensed	Licensed
Based standard	3GPP	IEEE 802.11p	Proprietary	Proprietary	3GPP	3GPP	ARIB STD-T103+119 IEEE 802.16n
Core network	Needed	Needed	Needed (LoRaWAN) Not Needed (LoRa)	Needed	Needed	Needed	Not Needed

systems. 4G and 5G primarily use the ultra-high-frequency (UHF) band and super-high-frequency (SHF) band, respectively, which facilitates a transmission distance of several kilometers per base station (BS). However, each BS requires a connection to the core network. Additionally, the use of public communication systems presents various problems, such as the huge subscriber fees owing to the requirement of up-to-date information from all the roads for nationwide use of V2X, in the cases such as automated driving. Therefore, a private wireless communication system, such as a wireless local area network (WLAN) with wide-area communication and without connection to a core network, is suitable for collecting information with a small number of BSs. Moreover, wireless communication must be standardized by the international standards development organizations.

IEEE 802.11p is a standard based on orthogonal frequency-division multiplexing (OFDM) for WLAN-based dedicated short-range communication systems (DSRCs) for vehicular communication; it is designed to support safety applications via V2X in 2010 [7]. Multihop communication is required to achieve long-range multicasting for full-range vehicular networks owing to the limited communication coverage of the IEEE 802.11p system [8]. However, its operating frequency is the 5 GHz band, which requires multiple hops to support an area of several tens of kilometers.

Several low-power wide-area (LPWA) communication systems for IoT devices have been analyzed in the sub-1 GHz band [3]. Additionally, private communications using licensed or unlicensed bands and 3GPP cellular-based public communications have also been analyzed. However, the bandwidth, associated transmission speed, mobility tolerance, and area range are restricted owing to the low power and wide area. In summary, no existing standardized system can ensure a communication distance of 10 km or more between BS and terminals; collect information from sensors, meters, and monitors, including moving images; and control them with transmission speeds above several Mbps in mobile environments, such as ITS and IoT.

These requirements can be satisfied by implementing the wireless regional area network (WRAN). WRAN is primarily employed for regional area communication over several tens of kilometers between wireless devices. It is mainly used in the VHF or UHF bands, such as the 200–400 MHz band, to secure a larger communication area per BS. One of the standardized WRAN systems is the IEEE 802.22 [9]. It was standardized in 2011; an initial prototype was developed [10] and demonstrated in the field [11]. However, IEEE 802.22 uses orthogonal frequency division multiple access (OFDMA) with a bandwidth of 6 MHz per channel, which is highly resistant to the frequency-selective fading that occurs in wide-area communications. This system is primarily intended for fixed communications and does not support mobile communications. Further research and development must be performed for commercialization in highly mobile environments [12] before it can be applied in ITSs.

IEEE 802.16 is a standard for broadband wireless communication systems based on OFDMA in higher UHF and SHF bands (recommended for application at 2.5, 3.5, and 5.8 GHz [13] in 2009). It was launched as Worldwide Interoperability for Microwave Access (WiMAX) [14]. Extensive research has been conducted in this field, and various studies have been conducted on the channel estimation methods [15], [16], [17]. It has a maximum carrier frequency of 5.8 GHz and a maximum speed of 100 km/h; the Doppler frequency is 537 Hz, and the cyclic prefix (CP) is set at approximately 10.0 μs [14]. Consequently, the system exhibits high resistance to movement speed (i.e., time fluctuation of the propagation channel) but not to the long-delayed waves (i.e., frequency selectivity).

ARIB STD-T103 was standardized for the WRAN system by the Association of Radio Industries and Businesses (ARIB) of Japan in 2011 to meet the formerly mentioned requirements [1], [18], [19]. In 2013, this standard was standardized as IEEE 802.16n (hereafter referred to as ARIB T103/IEEE 802.16n) [20]. This is a broadband mobile communication system that uses OFDMA in the VHF band for public usage. Wireless communication systems using the VHF band are characterized by less power attenuation over the same distance as compared to the UHF and higher bands. Therefore, a WRAN in the VHF band is expected to be used over a wide area of several tens of kilometers. Additionally, tolerance to the multipath fading that occurs in wide

communication areas can be expected owing to the usage of OFDMA. In terms of the size of fast Fourier transforms (FFTs) per channel, the number of ARIB T103/IEEE 802.16n (FFT size is 1024) is greater than or equal to that of IEEE 802.16-2009 because ARIB T103/IEEE 802.16n was developed based on IEEE 802.16-2019. Therefore, since the subcarrier spacing of ARIB T103/IEEE 802.16n is less than or equal to that of IEEE 802.16-2009, ARIB T103/IEEE 802.16n exhibits the same or higher resistance to frequency-selective fading as that exhibited by IEEE 802.16-2009. Furthermore, ARIB T103/IEEE 802.16n is specialized for the VHF band. Therefore, it is expected to have a longer transmission distance than IEEE 802.16-2009, which primarily uses frequencies above the UHF band. ARIB T103/IEEE 802.16n also requires a smaller FFT size than IEEE 802.22 (with an FFT size of 2048), making it relatively easy to build devices. Moreover, ARIB T103/IEEE 802.16n supports mobile communication with a transmission rate of several Mbps [1], [18], [20], which is not supported by IEEE 802.22, does not require a core network like IEEE 802.22, and is easier to install than 4G and 5G networks. Therefore, ARIB T103/IEEE 802.16n is expected to be an effective communication system for V2X to meet the requirement of super-large-coverage over 10 km and higher transmission rate over several Mbps. However, all the modulation schemes developed in previous studies [21], including uplink and downlink, with and without diversity, for ARIB T103/IEEE 802.16n were not comprehensively analyzed using computer simulations and experimental evaluations. Additionally, the transmission distance achieved using the ARIB T103/IEEE 802.16n has not been analyzed. This analysis of the transmission distance must also include an expansion of the transmission distance, assuming the relay between the relay stations (RSs).

In our previous shorter version study [1], we proposed a channel estimation method for ARIB T103/IEEE 802.16n downlink in a highly mobile environment to reduce the memory required for reception. The bit error rate (BER) performance was evaluated using 64 QAM-OFDM and maximum-ratio combining (MRC) diversity via computer simulations. Moreover, a prototype of ARIB T103/IEEE 802.16n was developed, and the transmission performance of the downlink was evaluated in a radio propagation environment in the VHF band [21]. This study is an extended version of our previous study, wherein we summarize the use cases and specifications of the ARIB T103/IEEE 802.16n system and comprehensively evaluate the transmission performance of both downlink and uplink in a VHF-band radio propagation environment through computer simulations and experimental evaluation using our WRAN prototype. In this evaluation, we employed both conventional and our proposed channel estimation methods. Subsequently, the transmission distance achieved using the ARIB T103/IEEE 802.16n was calculated based on the evaluation results. The main contributions of this study are summarized as follows:

- We formulated the use cases and specifications of the ARIB T103/IEEE 802.16n for IoT and V2X in the VHF band.
- In addition to the computer simulation and experimental evaluation results in [1] and [21], the transmission performance of ARIB T103/IEEE 802.16n with all the modulation schemes, uplink and downlink, and with and without diversity was comprehensively evaluated through computer simulations and experimental analysis of the transmission characteristics of the VHF band. The results of the computer simulation were validated based on the experimental results obtained from our WRAN prototype. Subsequently, the signal-to-noise ratio (SNR) and input power at the receiver required to achieve the BER of 10^{-6} were determined.
- The transmission distance between the RSs of ARIB T103/IEEE 802.16n with and without the multihop relay was evaluated by using the required input power obtained from the experimental evaluation.

The remainder of this article is organized as follows. Section II describes the use case and fundamental specifications of the ARIB T103/IEEE 802.16n standard. Section III presents a detailed description of the specifications of ARIB T103/IEEE 802.16n Mode 1. Section IV presents channel estimation and equalization schemes for DL and UL in ARIB T103/IEEE 802.16n Mode 1. Moreover, the enhanced scheme is proposed for DL. Sections V and VI present the computer simulation results and experimental laboratory results of ARIB T103/IEEE 802.16n Mode 1. Section VII describes the expected transmission distance based on the results. Lastly, Section VIII summarizes the conclusions drawn from the study.

II. USE CASE AND SPECIFICATION OF ARIB T103/IEEE 802.16N

A. USE CASE

Fig. 1 presents an example of the CPS platform using a WRAN and other wireless communication systems. When not using WRAN, the public wireless communication systems, and local-area private communication systems collect various types of information. For example, a public mobile communication system standardized by the 3GPP such as 5G is used for public communication. A wireless smart ubiquitous network (Wi-SUN) standardized by IEEE 802.15.4g [22] or a WLAN by IEEE 802.11 is used for local-area private communication. However, the communication service area is only a public operator's service area, which expands through local communication. In addition, using these services incurs subscriber fees. These issues increase the difficulty of installing existing systems. On the contrary, the WRAN system conforming to ARIB STD-T103 can cover a wide range of 10 km or more with a transmission rate of several Mbps. Thus, we envision three use cases for WRAN: 1) IoT communications, 2) mobile communications, and 3) V2X communications.

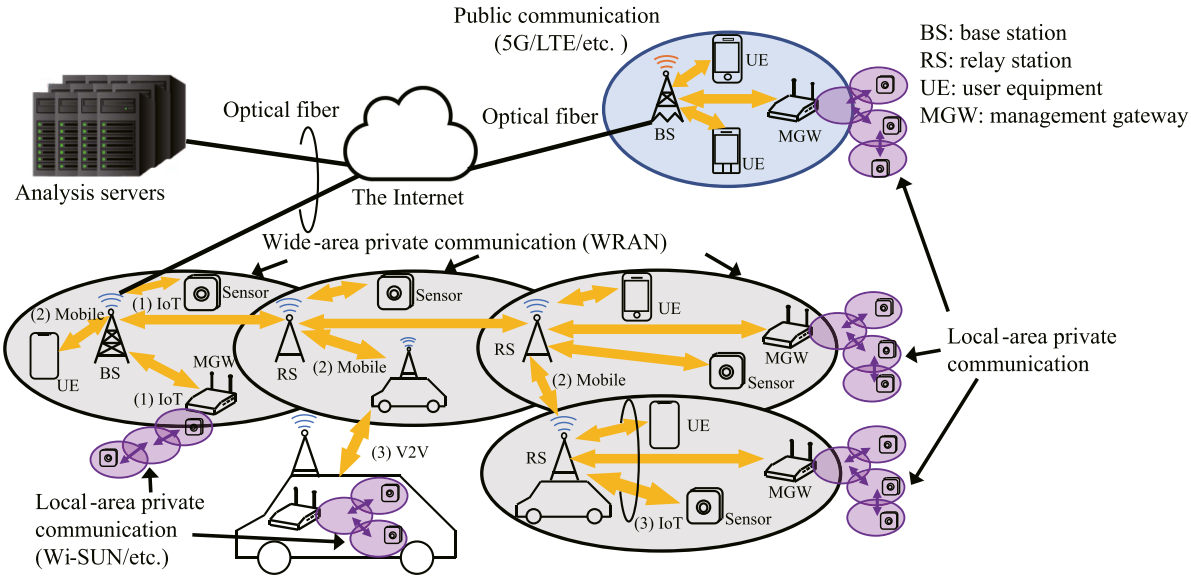

FIGURE 1. Example of public and private wireless communication systems on the CPS platform.

1) IOT COMMUNICATIONS

Various types of information, such as sensor data, are collected from the wide area with a distance of 10 km or more supported by the WRAN systems. We assume that the communication is performed directly using the sensor data with WRAN and the data is collected in the local area using another communication system (such as Wi-SUN or WLAN) and transmitted with WRAN via a management gateway (MGW). In V2X, communication is categorized as vehicle-to-infrastructure (V2I). It is expected to be used in various fields, such as a collection of information from both the environment and road monitoring sensors [3].

2) MOBILE COMMUNICATIONS

For mobile communications, we assume that communication is performed with moving user equipment (UE), similar to general public cellular communication and communication with vehicles, such as cars. In the vehicle, various control information required for automatic driving and other actions, is collected locally via Wi-SUN or WLAN, etc., and this information is widely collected via WRAN. Conversely, WRAN can be used to remotely achieve the control required for automated driving. V2X communication is categorized as vehicle-to-network (V2N).

3) V2V AND IAB COMMUNICATIONS

When a vehicle is outside the WRAN communication area, the communication area is extended using multihop communication via vehicle-to-vehicle (V2V) communication [23] based on the WRAN. Moreover, the communication area can be expanded as an integrated access and backhaul (IAB) link by installing a WRAN BS, which functions as an RS in a vehicle. For example, it can function as a temporary BS in the event of a disaster. This RS can be connected to terminals using WRAN and can also transmit information collected by Wi-SUN and WLAN using the MGW function of RS.

B. SPECIFICATION

The ARIB STD-T103 [18] was standardized for WRAN systems by the ARIB in Japan in 2011. The ARIB STD-T103 is a broadband mobile communication system which employs OFDMA in the VHF band for public usage. Wireless communication systems using the VHF band are characterized by less power attenuation for the same distance as the UHF and higher bands. Consequently, a WRAN in the VHF band is expected to be used over a wide area, such as several tens of kilometers. Table 2 lists the specifications of ARIB STD-T103. The ARIB STD-T103 operates with a bandwidth of 5 MHz per channel and has two modes: Mode 1 and Mode 2. Mode 1 has two FFT size options: 512 and 1024-point FFTs. The modulation schemes, duplex methods, multiple access schemes, maximum transmission (Tx) power, and medium access control (MAC) layer protocol of Mode 1 are based on IEEE 802.16-2009 [16]. In IEEE 802.16-2009, 1024-point FFTs are not supported for the operation of a 5 MHz bandwidth. However, 1024 FFTs can be used even in operation with a 5 MHz bandwidth to compensate for signal variations due to severe frequency-selective fading in the VHF band.

The differences between the 512 and 1024-point FFT systems are in terms of the following: FFT size, frame length, OFDM symbol length, and CP length. In this study, we focused only on the 1024-point FFT-applied Mode 1 owing to its widespread usage in Japan [21]. As the 1024-point FFT-applied systems achieve a CP of over 20 μs, they can support delayed paths of greater than 20 μs. In addition to the above differences, Mode 1 has unique pilot patterns between the downlink (DL) and uplink (UL) to compensate for signal variations that are caused by fading and the slot allocation ratio for the DL and UL in a time-division duplex (TDD)

TABLE 2. Specification of ARIB STD-T103

	Parameter							
Base standard	Wireless MAN-OFDMA (IEEE 802.16-2009)							
Channel bandwidth	5.0 MHz (4.9 MHz occupied)							
Modulation scheme	QPSK, 16QAM, and 64QAM							
Duplex method	Time division duplex (TDD)							
Multiple access	DL: OFDM/time division multiplexing (TDM), UL: OFDMA							
Transmission (Tx) power	5 W (37 dBm)							
Mode	Mode 1					Mode 2		
FFT size	512 point		1024 point					
Subcarrier spacing	10.94 kHz		5.47 kHz					
Frame length	5.0 ms		10 ms					
OFDM symbol length	102.8 µs		205.7 µs					
CP length (ratio:1/8)	11.4 µs		22.9 µs					
Symbol rate (T_s)	9.728 kHz		4.862 kHz					
Ratio of DL to UL symbols	35:12	26:21	35:12	26:21	9:38	37:10	23:24	9:38
Number of symbols for control	DL: 6 symbols, UL: 3 symbols							
Maximum throughput (T_x^{max}) for DL* (Mbps)	6.3	4.3	6.3	4.3	0.65	5.9	3.2	0.57
Maximum throughput (T_x^{max}) for UL* (Mbps)	1.5	3.0	1.5	3.0	5.9	1.5	4.5	7.6
Pilot pattern	IEEE 802.16-2009					ARIB STD-T103 original		
MAC	IEEE 802.16-2009					ARIB STD-T103 original		

*when 64QAM and coding rate of 1/2 are used.

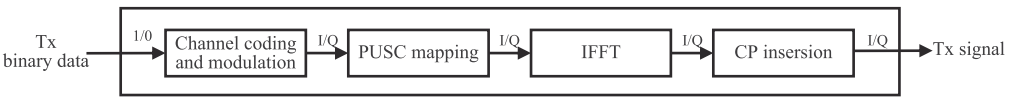

FIGURE 2. Structure of transmitter.

TABLE 3. Average Number of Subcarriers

	Mode 1		Mode 2	
	DL	UL	Dl	UL
Null subcarriers	184			
Pilot subcarriers	120	280	210	120
Data subcarriers	720	560	630	720

frame [18]. Mode 1, with a 512-point FFT, could support only 35:21 and 26:21, respectively. However, with a 1024-point FFT, Mode 1 supported a different ratio of 9:38. Mode 2 supported ratios of 37:10, 23:24, and 9:38. Therefore, Mode 1 with the 1024-point FFT, and Mode 2 can provide a higher ratio of UL and are effective in various cases, such as monitoring, metering, and surveillance. The pilot patterns of ARIB STD-T103 are roughly divided into the cluster and tile types [1], [18]. In the tile type, pilot subcarriers are placed at the four corners of each resource unit, whereas in the cluster type, they are not placed at the four corners. Cluster and tile types differ in transmission speed owing to the number of pilot subcarriers, resistance to frequency selectivity, and resistance to time fluctuations. Table 3 lists the average numbers of null, pilot, and data subcarriers for each OFDM symbol. The ARIB STD-T103 in 2011 and IEEE 802.16-2009 were standardized to IEEE 802.16n in 2013 [20].

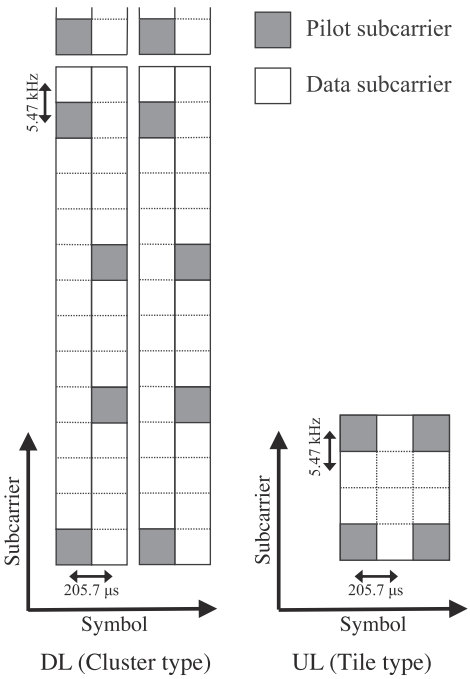

FIGURE 3. Pilot patterns of mode 1.

III. MODE 1 SPECIFICATIONS OF TRANSCEIVER

A. TRANSMITTER

Fig. 2 depicts the transmitter block diagram of the ARIB T103/IEEE 802.16n system and the process of each block is presented in [1]. The transmitter performs channel coding, modulation, frequency interleave using partial usage subchannelization (PUSC), inverse FFT (IFFT), and OFDM processes, including CP. The frequency interleave and CP increased the resistance to long delay paths. Mode 1 uses pilot allocations standardized in IEEE 802.16-2009, as shown in Fig 3. DL uses cluster-type channel allocation combined with

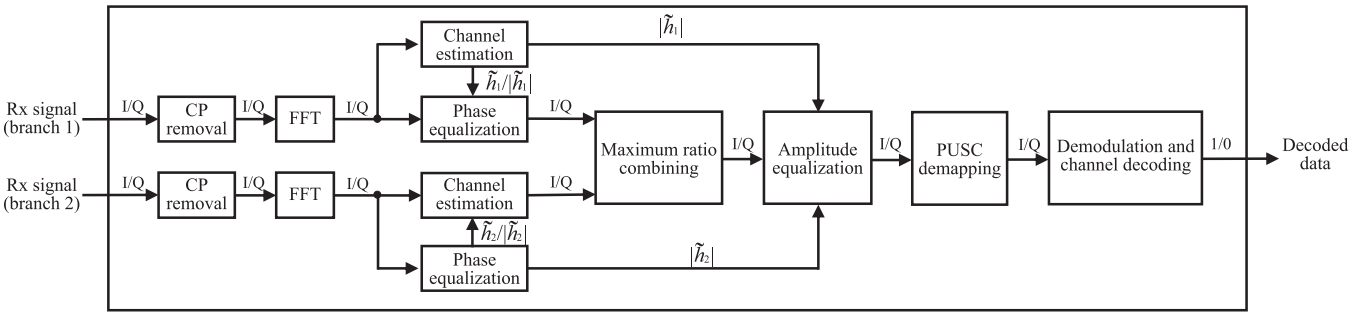

FIGURE 4. Structure of proposed receiver with MRC diversity.

a high data symbol ratio, leading to the difficulty of estimation. Conversely, UL uses a tile-type channel allocation set with a low data symbol ratio, which makes channel estimation relatively easy.

B. RECEIVER

Fig. 4 shows the proposed receiver block diagram of a ARIB T103/IEEE 802.16n system [1]. First, each CP is removed before obtaining the received subcarriers through FFT processing. If the CP length is sufficient for removing the effect of the delay paths, there is no inter-symbol interference (ISI) or inter-carrier interference (ICI) in the obtained subcarriers. Subsequently, the receiver performs channel estimation, equalization, demapping using PUSC, demodulation, and channel decoding. Fig. 4 depicts the receiver block diagram of the MRC diversity [24]. It was assumed that the MRC diversity could be applied to two receiving antennas. By employing the received signal (r_1) and estimated effective channel ($\tilde{h}_1$) of branch 1, and the received signal (r_2) and estimated effective channel ($\tilde{h}_2$) of branch 2, the MRC-processed and equalized signal, r', can be obtained as follows:

$$r' = \frac{r_1\tilde{h}_1^* + r_2\tilde{h}_2^*}{|\tilde{h}_1|^2 + |\tilde{h}_2|^2}, \tag{1}$$

where $*$ denotes complex conjugate.

IV. CHANNEL ESTIMATION AND EQUALIZATION

This section presents the basic channel estimation and equalization schemes for DL and UL in ARIB T103/IEEE 802.16n Mode 1. Moreover, the enhanced scheme is proposed for DL. The received subcarriers are expressed as follows:

$$r_{i,j} = h_{i,j}s_{i,j} + n_{i,j}, \tag{2}$$

where $s_{i,j} \in \mathbb{C}$, $r_{i,j} \in \mathbb{C}$, $h_{i,j} \in \mathbb{C}$, and $n_{i,j} \in \mathbb{C}$ represent the transmitted signal, received signal, effective channel, and noise signal of the j-th subcarrier in the i-th OFDM symbol, respectively. The effective channels, $\hat{h}_{p,q_p}$, can be obtained by employing the transmitted and received signals of the pilot subcarriers, as follows:

$$\hat{h}_{p,q_p} = \frac{r_{p,q_p}}{s_{p,q_p}} = h_{p,q_p} + \frac{n_{p,q_p}}{s_{p,q_p}}, \tag{3}$$

where q_p represents the pilot subcarrier index in the p-th OFDM symbol. The transmitted signals are known from both the transmitter and receiver. The effective channel, $\tilde{h}_{i,j}$, of the data subcarriers is estimated by using the obtained effective channels of the pilot subcarriers, $\hat{h}_{p,q_p}$. To equalize the effective channel and obtain the transmitted signals $s_{i,j}$, the received signals, $r_{i,j}$, were divided by the estimated effective channel, $\tilde{h}_{i,j}$. The following subsections present the schemes used to estimate the channels of data symbols from the estimated channels of pilot symbols per pilot allocation.

A. CHANNEL ESTIMATION SCHEMES FOR DL (CLUSTER TYPE)

The three pilot subcarriers were not arranged at the corner of the cluster type in DL, as shown in Fig. 3. Therefore, the effective channels of the data subcarriers that were not allocated between the pilot subcarriers were estimated using the incomplete scheme using pilots of the adjacent clusters in the conventional scheme [15], [16], as shown in Fig. 5(a). However, storing information other than the subcarriers of the user cluster is necessary to use the pilot subcarriers of the adjacent clusters, thereby squeezing the hardware memory. Therefore, a complete scheme for the DL cluster structure was proposed, as shown in Fig. 5(b), [1]. The conventional and proposed schemes were applied in the time and frequency-domain estimation stages.

Let the effective channel in each cluster be defined as $\tilde{h}_{s,t}^{x,z} = \hat{h}_{i,j}$, where $s = i \bmod 2$ and $t = j \bmod 14$ are the symbol and subcarrier indices, respectively, and $x = i/2$ and $z = j/14$ are the cluster symbol and subcarrier indices.

First, we describe the time-domain estimation stage. In the conventional scheme, the effective channels of two adjacent symbols in one cluster are estimated by interpolating those of both the pilots of the cluster and the adjacent cluster, as follows:

$$\begin{aligned} \tilde{h}_{1,t}^{x,z} &= \frac{1}{2}\left\{\tilde{h}_{0,t}^{x,z} + \tilde{h}_{0,t}^{x+1,z}\right\} \quad (t = 0,\ 12), \\ \tilde{h}_{0,t}^{x,z} &= \frac{1}{2}\left\{\tilde{h}_{1,t}^{x,z} + \tilde{h}_{1,t}^{x-1,z}\right\} \quad (t = 4,\ 8). \end{aligned} \tag{4}$$

However, we assumed these effective channels were identical in the proposed scheme. The adjacent effective channels

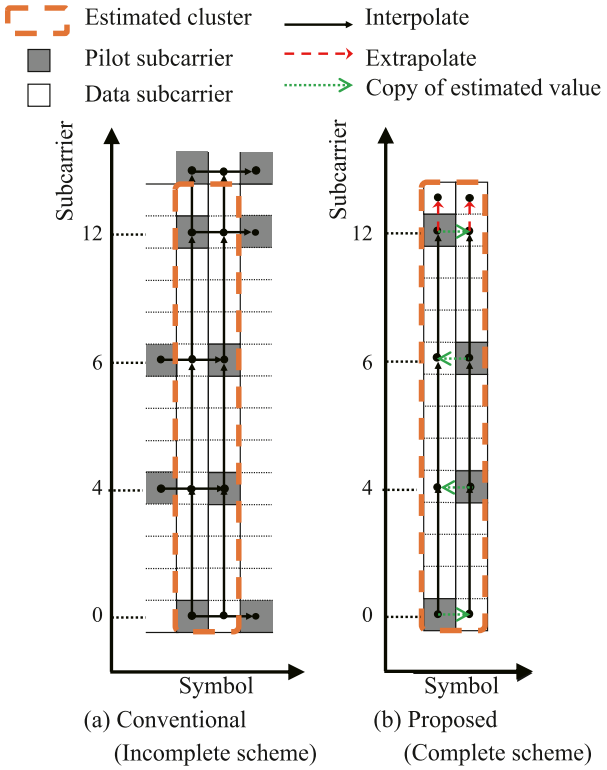

FIGURE 5. Channel estimation schemes for DL (cluster type).

of the pilots in the time domain were estimated by copying the estimated effective channels of the pilots as follows:

$$\begin{aligned} \tilde{h}^{x,z}_{1,t} &= \tilde{h}^{x,z}_{0,t} \quad (t = 0,\ 12)\,, \\ \tilde{h}^{x,z}_{0,t} &= \tilde{h}^{x,z}_{1,t} \quad (t = 4,\ 8)\,. \end{aligned} \tag{5}$$

Next, we describe the frequency-domain estimation stage. In both the schemes, all the effective channels of the data subcarriers, except the 13th subcarrier, were estimated by interpolating between the pilots of their cluster, as follows:

$$\tilde{h}^{x,z}_{s,t} = \frac{1}{4}\left\{t_{\mathrm{mod}}\tilde{h}^{x,z}_{s,4(\lfloor \frac{t}{4} \rfloor+1)} + (4 - t_{\mathrm{mod}})\,\tilde{h}^{x,z}_{s,4\lfloor \frac{t}{4} \rfloor}\right\}(t = 13)\,, \tag{6}$$

where $t_{\mathrm{mod}} = t \bmod 4$.

In the proposed scheme, the effective channel of the 13th subcarrier is estimated by extrapolating from the estimated effective channels of the 8th and 12th subcarriers, as follows:

$$\tilde{h}^{x,z}_{s,13} = \frac{1}{4}\left\{5\tilde{h}^{x,z}_{s,12} - \tilde{h}^{x,z}_{s,8}\right\}. \tag{7}$$

However, in the conventional scheme, the effective channel of the 13th subcarrier was estimated by interpolating the estimated effective channels of the 12th subcarrier of the cluster and the 1st subcarrier of the adjacent cluster as follows:

$$\tilde{h}^{x,z}_{s,13} = \frac{1}{2}\left\{\tilde{h}^{x,z+1}_{s,0} - \tilde{h}^{x,z}_{s,12}\right\}. \tag{8}$$

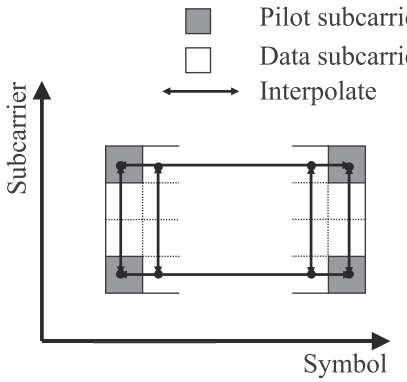

FIGURE 6. Channel estimation scheme for UL (tile type).

B. CHANNEL ESTIMATION SCHEMES FOR UL (TILE TYPE)

There are few channel estimation considerations for the tile type because the pilot subcarriers are arranged at the four corners and bracket all the data subcarriers. An estimation scheme equivalent to the complete scheme was proposed in IEEE 802.16-2009 [17].

As all the pilot subcarriers are allocated to the corners, the effective channels of the data subcarriers can be estimated by interpolating those of the pilot subcarriers, as shown in Fig. 6. Therefore, the incomplete scheme is not useful for the tile type, regardless of DL/UL. The number of symbols per tile is defined as k. The effective channel in each tile is defined as $\tilde{h}^{x,z}_{s,t} = \hat{h}_{i,j}$, where $s = i \bmod k$ and $t = j \bmod 4$ are the symbol and subcarrier indices in each tile, respectively, and $x = i/k$ and $z = j/4$ are the tile symbol and subcarrier indices. All the effective channels of the data subcarriers were estimated by interpolating between those of the pilot subcarriers in the frequency and time domains as follows:

$$\begin{aligned} \tilde{h}^{x,z}_{s,t} = \frac{1}{3\,(k-1)}\Big\{&(k-s-1)\,(3-t)\,\tilde{h}^{x,z}_{0,0} + st\tilde{h}^{x,z}_{2,3} \\ &+ s\,(3-t)\,\tilde{h}^{x,z}_{2,0} + (k-s-1)\,t\,\tilde{h}^{x,z}_{0,3}\Big\} \end{aligned} \tag{9}$$

V. MODE 1 PERFORMANCE ANALYSIS BY COMPUTER SIMULATION

The transmission performance of Mode 1 in the ARIB T103/IEEE 802.16n was evaluated through computer simulation in terms of E_b/N_0 to BER. The proposed and conventional channel estimation schemes were compared and evaluated. The computer simulation codes were developed from scratch using MATLAB [25], and no communication-specific toolbox was used. Table 4 lists the simulation parameters. The additive white Gaussian noise (AWGN) environment, typical GSM urban model, and IEEE 802.22 Profile A model were used for the evaluation. Tables 5 and 6 list the models. The IEEE 802.22 Profile A model is a multipath fading channel model with a long delay path for a service distance of 10 km, standardized by the IEEE 802.22 working group. The required BER was set to 10^{-6} on ARIB STD-T103 [18].

TABLE 4. Configurations of Evaluation Parameters

	Computer simulation	Experimental evaluation
Standard	ARIB STD-T103 (Mode 1)	
Channel model	AWGN environment GSM Typical Urban model IEEE 802.22 Profile A model	
Encoding and decoding	Convolutional turbo codes (coding rate: 1/2) and Max-Log MAP algorithm	
Moving speed	80 km/h ($f_D T_s = 3 \times 10^{-3}$)	
DL:UL ratio	N/A	9:38
Max Tx power		37 dBm (BS),
Frequency		192.5 MHz -197.5 MHz

TABLE 5. GSM Typical Urban Model

Path number	1	2	3	4	5	6
Delay time [μs]	−0.2	0	0.3	1.4	2.1	4.8
Relative power [dB]	−3.0	0	−2.0	−6.0	−8.0	−10

TABLE 6 IEEE 802.22 Profile A Model

Path number	1	2	3	4	5	6
Delay time [μs]	0	3.0	8.0	11	13	21
Relative power [dB]	0	−7.0	−15	−22	−24	−19

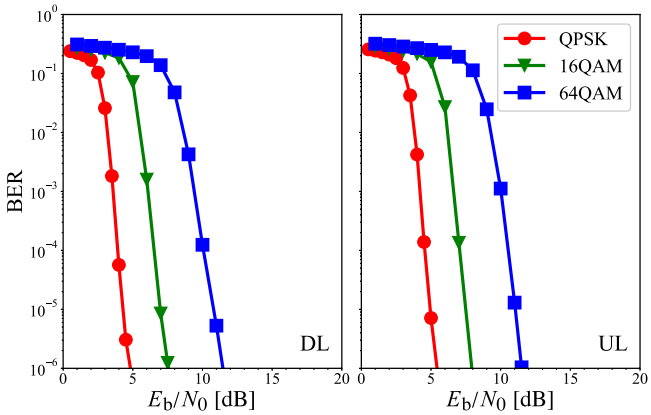

FIGURE 7. Performance evaluation in AWGN environment.

A. PERFORMANCE ANALYSIS IN AWGN ENVIRONMENT

Fig. 7 depicts the BER performance of Mode 1 in an AWGN environment for each modulation scheme. The DL and UL exhibited nearly identical performances. Table 7 lists the E_b/N_0 and SNR of each modulation scheme that achieved the required BER $= 10^{-6}$. The difference in the E_b/N_0 is up to 6 dB. The performance difference for each mode was caused by the difference between the number of data subcarriers and boost of the pilot subcarriers.

B. COMPARISON OF CHANNEL ESTIMATION SCHEMES IN MULTIPATH FADING ENVIRONMENT

Fig. 8 depicts the BER performance of the receiver using two channel estimation schemes for DL and a channel estimation scheme for UL when compared to the ideal case with 64QAM in a typical GSM urban model. The BER degradation of

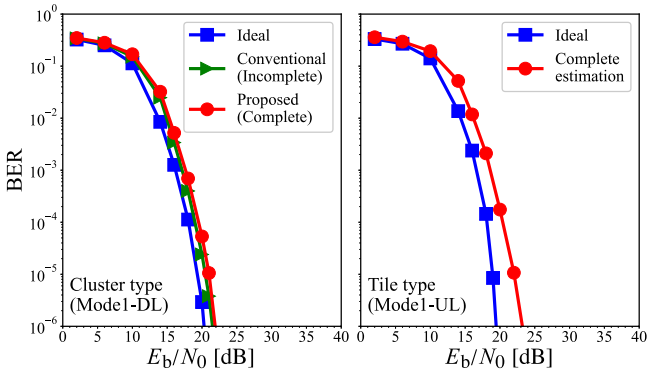

FIGURE 8. Performance evaluation of channel estimation schemes with 64 QAM in typical urban model.

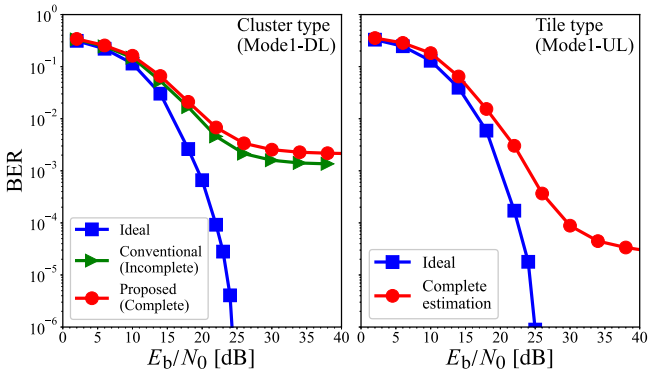

FIGURE 9. Performance evaluation of channel estimation schemes with 64 QAM in 802.22 profile A model.

the proposed scheme is up to 3.0 dB when compared to the ideal case in terms of E_b/N_0 at BER $= 10^{-6}$. Consequently, the channel estimation error slightly degrades the BER performance of a typical GSM urban model. In addition, the complete DL scheme exhibited almost no deterioration when compared to the conventional scheme.

Fig. 9 shows the BER performance of the receiver using the channel estimation schemes in the IEEE 802.22 Profile A model. An error floor was observed both the DL estimation schemes. The proposed scheme showed a slightly higher error floor than the conventional scheme and was adopted as the most straightforward scheme in the following discussion. Similarly, UL showed an error floor. This is because a wider pilot subcarrier interval induces a more significant channel estimation error owing to the severe frequency selectivity of fading caused by a long delay.

C. COMPARISON OF MODULATION SCHEMES IN MULTIPATH FADING ENVIRONMENT

Fig. 10 depicts the BER performance of Mode 1 in a typical GSM urban model for each modulation scheme based on the proposed channel estimation scheme. Similar characteristics are observed in DL and UL owing to the relatively high channel estimation accuracy. Table 7 also lists the E_b/N_0 and SNR of each modulation scheme that achieved the required

TABLE 7. Required E_b/N_0 and SNR [dB] to Achieve the Required BER=10^{-6} in Computer Simulation

	AWGN		TU		Profile A		Profile A w/ div.	
	DL	UL	DL	UL	DL	UL	DL	UL
QPSK	5.0/3.3	5.5/2.7	18/16	18/15	26/25	22/20	14/12	14/11
16QAM	7.5/8.8	8.0/8.2	20/21	21/21	N/A	26/26	17/19	16/16
64QAM	12/15	11.5/14	22/25	24/26	N/A	N/A	28/31	20/22

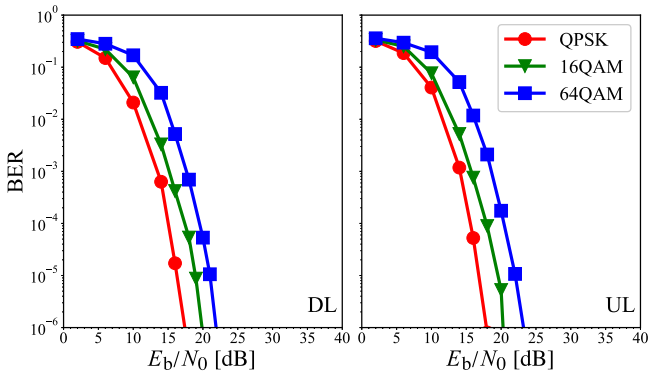

FIGURE 10. Performance evaluation in typical urban model.

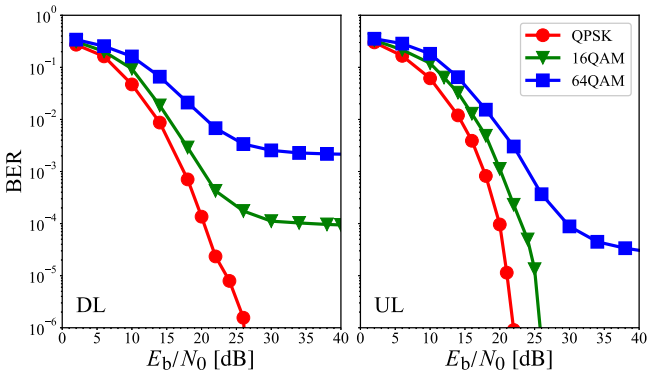

FIGURE 11. Performance evaluation in 802.22 profile A model.

BER $= 10^{-6}$ in multipath fading environment. Similar to the AWGN environment, the difference for each modulation scheme of the E_b/N_0 that achieves the required BER $= 10^{-6}$ is up to 6 dB.

Fig. 11 depicts the BER performance of the IEEE 802.22 Profile A model obtained through computer simulation for each modulation scheme. An error floor occurs under all conditions in 64QAM, as explained earlier. In DL, an error floor also occurs in 16QAM, and the performance in QPSK is significantly degraded when compared to UL. Therefore, the UL affords several advantages in a VHF-band transmission environment when using a single antenna. Additionally, 16QAM and 64QAM transmissions are difficult in the VHF transmission environments with long delay paths.

D. COMPARISON OF MRC DIVERSITY IN MULTIPATH FADING ENVIRONMENT

Fig. 12 depicts the BER performance using the MRC diversity in the IEEE 802.22 Profile A model. The tendency of

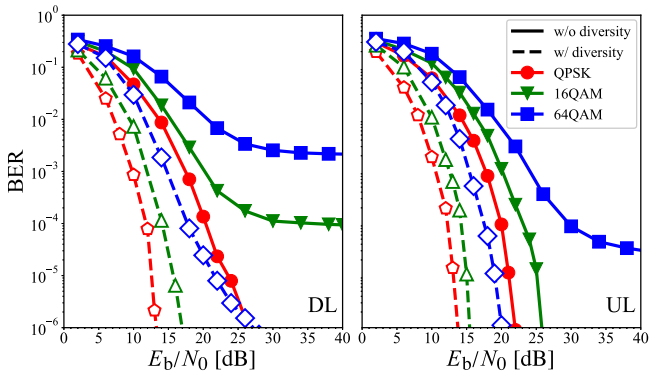

FIGURE 12. Performance evaluation in 802.22 profile A model with MRC diversity.

the error floor appears slightly in 64QAM with DL (cluster type); however, high-quality transmission can be achieved with the tile types. These tendencies demonstrate that high-speed transmission can be achieved using the two branches of MRC diversity. Table 6 also lists the E_b/N_0 and SNR of each modulation scheme that achieved the required BER $= 10^{-6}$.

VI. MODE 1 EXPERIMENTAL PERFORMANCE ANALYSIS BY PROTOTYPE

The transmission performances of the transceivers using Mode 1 were evaluated through laboratory experiments using prototypes in terms of the input power to the BER. The experimental evaluation used parameters shown in Tables 3 and 4 and Fig. 13 shows our developed prototype and the experimental evaluation setup [21]. In the developed prototype, the proposed channel estimation method for downlink is implemented. The AWGN environment, typical GSM urban model, and IEEE 802.22 Profile A model were used for the evaluation.

A. PERFORMANCE ANALYSIS IN AWGN ENVIRONMENT

This subsection presents the evaluation of the prototype in the AWGN environment. Fig. 14 depicts a diagram of the experimental evaluation of the prototype. The DL and UL were evaluated using different diagrams. The device was equipped with the 1st antenna for transmission and reception and the 2nd antenna for reception.

Fig. 15 displays the BER performance in the AWGN environment obtained in the experimental evaluation for each modulation scheme. Both the receiving antennas were evaluated. The BER of the1st antenna was degraded by 1.5–2.0 dB in terms of SNR at BER $= 10^{-6}$ compared to the 2nd antenna because the signal power required to reach the processing unit

(a) Developed prototype (right: BS, left: MS)

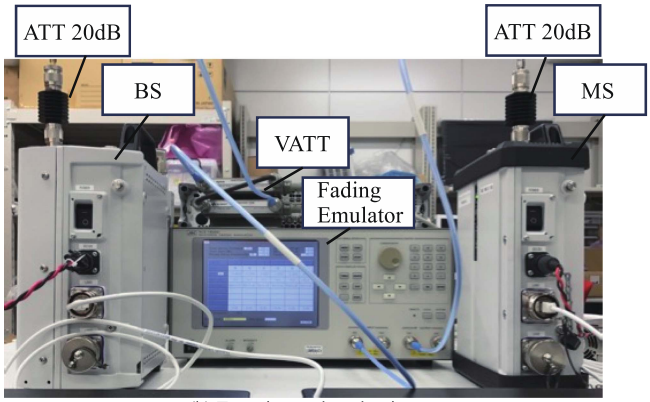

(b) Experimental evaluation setup

FIGURE 13. Developed prototype and experimental evaluation setup [21].

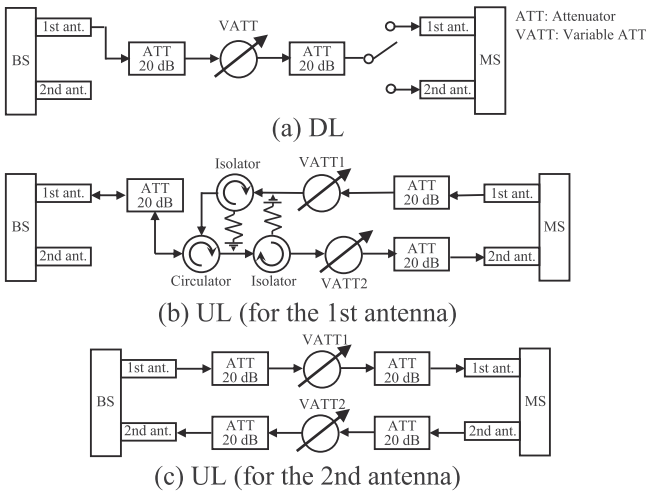

FIGURE 14. Experimental evaluation in AWGN environment.

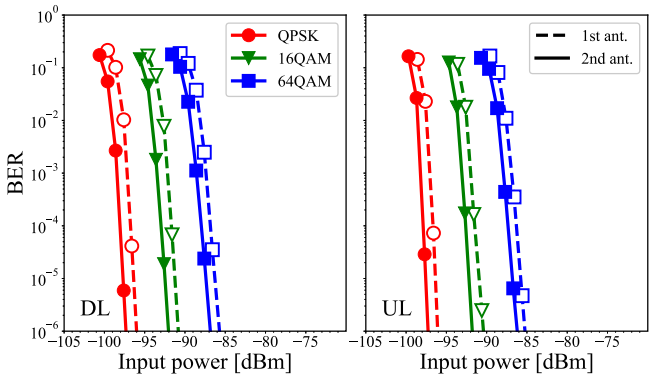

FIGURE 15. Experimental evaluation in AWGN environment.

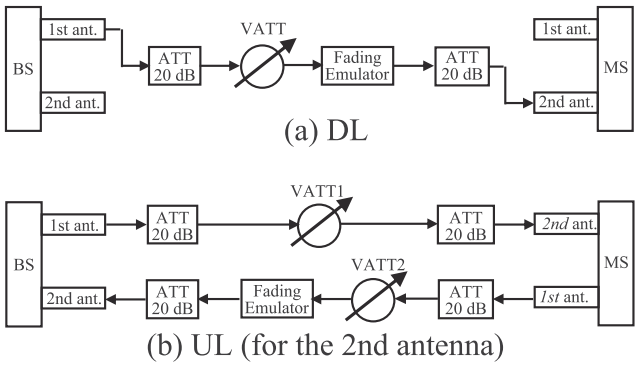

FIGURE 16. Experimental evaluation in multipath fading environment.

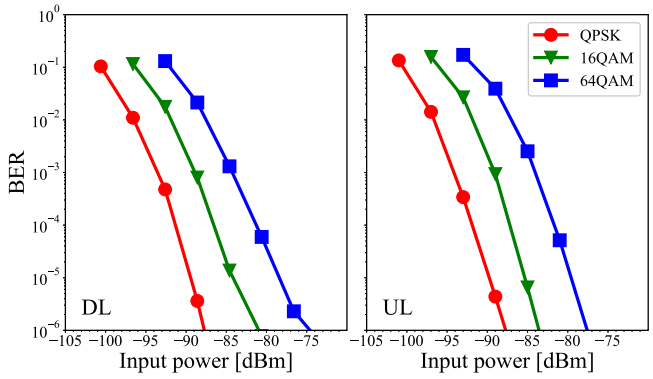

FIGURE 17. Experimental evaluation in typical urban model.

is different due to power attenuation by the circulation processing of 1st antenna, even if the power input to the antenna is identical. Only the 2nd antenna was used for the subsequent evaluation with a single antenna. The BER characteristics exhibited an almost identical slope for both the experiments and computer simulations.

Table 8 lists the input power required to achieve the required BER $= 10^{-6}$. In the AWGN environment, the performance of DL and UL was nearly identical. The difference for each MCS in the input power that achieves the required BER $= 10^{-6}$ is approximately 5–6 dB and is almost identical to that of a computer simulation. These results demonstrate the validity of the computer simulation in this environment.

B. COMPARISON OF MODULATION SCHEMES IN MULTIPATH FADING ENVIRONMENT

In this subsection, we present an evaluation of the performance of the prototype in a multipath fading environment through laboratory experiments by using a fading emulator (JRC, NJZ-1600D). Fig. 16 presents a diagram of the experimental evaluation performed using the prototype and fading emulator. The prototype used in this experiment was installed using the complete proposed scheme for channel estimation.

TABLE 8. Required Input Power [dBm] to Achieve the Required BER=10^{-6} by Experimental Evaluation

	AWGN		TU		Prof. A		Prof. A w/ div.	
	DL	UL	DL	UL	DL	UL	DL	UL
QPSK	–97	–97	–87	–87	N/A	–74	–87	–86
16QAM	–92	–91	–81	–83	N/A	N/A	–83	–81
64QAM	–87	–86	–74	–77	N/A	N/A	N/A	–74

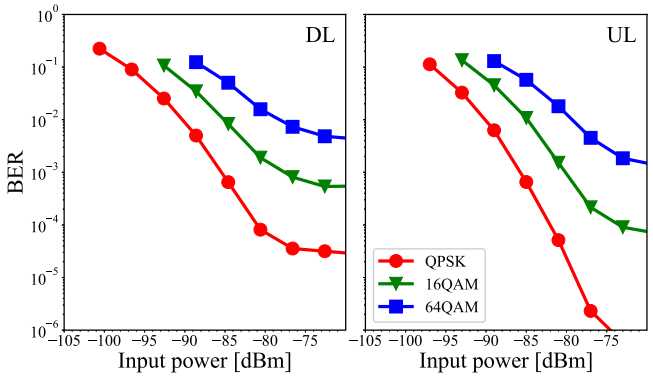

FIGURE 18. Experimental evaluation in 802.22 profile A model.

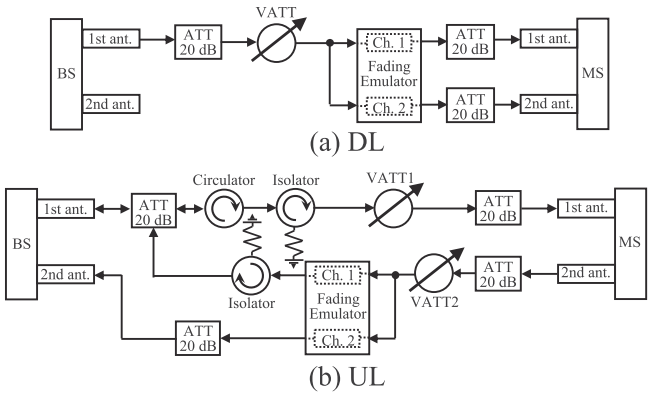

FIGURE 19. Experimental evaluation with MRC diversity in multipath fading environment.

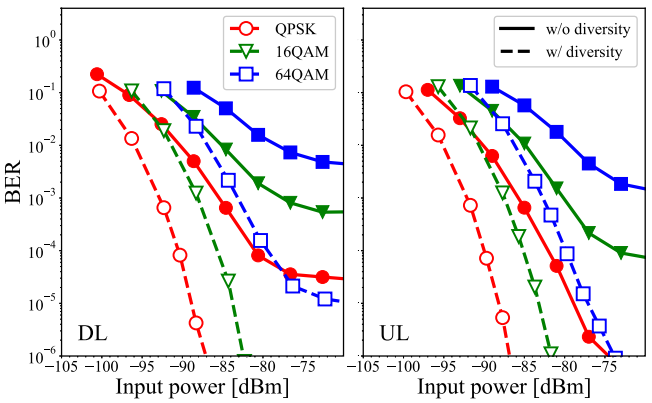

FIGURE 20. Experimental evaluation in 802.22 Profile A model with MRC diversity.

Fig. 17 depicts the BER performance in a typical GSM urban model obtained through experimental evaluation for each modulation scheme. Table 8 also lists the input power required to achieve the required BER $= 10^{-6}$ in the multipath fading environment. The difference between each MCS of the input power, which achieves the required BER $= 10^{-6}$, is almost identical to that of a computer simulation. These results demonstrate the validity of the computer simulation in this environment. Similarly, Fig. 18 depicts the BER performance of the IEEE 802.22 Profile A model through an experimental evaluation for each modulation scheme. The tendency of the error floor is observed slightly in all the modulation schemes with DL (cluster type) and in 16QAM and 64QAM with UL (tile type). Table 8 also lists the input power required to achieve the required BER of each modulation scheme's required BER $= 10^{-6}$ in the multipath fading environment. In the experimental evaluation, the performance was slightly degraded when compared to the computer simulation. However, a similar tendency is observed when DL (cluster type) performs better than UL (tile type). These results verify the validity of the computer simulation in this environment.

C. COMPARISON OF MRC DIVERSITY IN MULTIPATH FADING ENVIRONMENT

We evaluated the performance of the prototype in multipath fading environments based on laboratory experiments using MRC diversity. Fig. 19 presents a diagram of the experimental evaluation performed using MRC diversity. Fig. 20 depicts the BER performance using MRC diversity in the IEEE 802.22 Profile A model through an experimental evaluation. The error floor disappeared in most modulation schemes and appeared slightly in 64QAM with DL (cluster-type). Based on these tendencies, it was confirmed that high-speed transmission can be achieved using two branches of MRC diversity. Table 8 also lists the input power required to achieve the required BER $= 10^{-6}$ for each modulation scheme in this evaluation.

VII. TRANSMISSION CAPABILITY OF MODE 1

We evaluated the transmission capacity by evaluating throughput based on the experimental results presented in Section VI. We evaluated both the single- and multihop transmissions.

A. DEFINITION OF THROUGHPUT

First, the throughput (T) of a single-hop transmission is defined as follows:

$$T = T^{\max}(1 - PER), \tag{10}$$

where $T^{\max}$ represents the maximum throughput as shown in Table 2 and PER is defined as $PER = 1 - (1 - BER)^{11200}$. The size of the maximum transmission unit that is used for WiMAX is 11200 [14]. Based on this equation, the input power versus T is evaluated using the evaluation results in Section V. Similarly, this clause defines the throughput of multihop transmission. Ideal regenerative repeaters were assumed, and the input power versus T was evaluated. It is assumed that the relay is repeated with the required input power, as shown in Table 8, where there is no degradation in the throughput and transmission can be achieved between terminals using $T^{\max}$. When transmitted by n-hop one to one relay, the transmission speed T^n is expressed as follows [26]:

$$T^n = \frac{T^{\max} n}{\sum_{k=1}^{n} k} = \frac{2T^{\max}}{n+1}. \tag{11}$$

B. EVALUATION OF THROUGHPUT

We evaluated the transmission distance versus throughput with the assumption of an actual operation. In this evaluation, the single-hop or multihop communication between RSs illustrated in Fig. 1 is considered as a use case. The RS antenna height, H_{RS}, is set to 3.0 m because the antenna is to be installed on the roof of a car. Table 4 lists the transmission powers, and the DL:UL ratio was assumed to be 9:38. This is because the control and sensor information from the car is transmitted to the cloud. In the evaluation, we use the Extended Hata model [27] as a path model. The path loss, L_d, at a transmission distance (d) of more than 0.1 km and less than 20 km is expressed as follows:

$$\begin{aligned}
L_d &= \begin{cases} L_d^{\mathrm{urban}}, & (\text{for TU model}) \\ L_d^{\mathrm{suburban}}, & (\text{for Prof. A model}) \end{cases}, \\
L_d^{\mathrm{urban}} &= 69.6 - 2a\left(H_{\mathrm{RS}}\right) \\
&\quad + 26.2\log\left(200\right) - 13.82\log\left(\max\left\{30, H_{\mathrm{RS}}\right\}\right) \\
&\quad + \left[44.9 - 6.55\log\left(\max\left\{30, H_{\mathrm{RS}}\right\}\right)\right]\log\left(d\right), \\
a\left(H_{\mathrm{RS}}\right) &= \left(1.1\log\left(200\right) - 0.7\right)\min\left\{10, H_{\mathrm{RS}}\right\} \\
&\quad - \left(1.56\log\left(200\right) - 0.8\right) + \max\left\{0, 20\log\left(\frac{H_{\mathrm{RS}}}{10}\right)\right\}, \\
L_d^{\mathrm{suburban}} &= L_d^{\mathrm{urban}} \\
&\quad - 2\left\{\log\left[\frac{\min\left\{\max\left\{150, 200\right\}, 2000\right\}}{28}\right]\right\}^2 - 40.94.
\end{aligned} \tag{12}$$

The path loss for the urban and suburban environments is used in the GSM Typical Urban model and IEEE 802.22 Profile A model, respectively. The input power at the receiver ($P_{\mathrm{R}}^{\mathrm{input}}$) in dBm is expressed as follows:

$$P_{\mathrm{R}}^{\mathrm{input}} = P_{\mathrm{T}} + G_{\mathrm{T}} + G_{\mathrm{R}} - L_d, \tag{13}$$

where P_{T}, G_{T}, and G_{R} represent the transmit power, transmitter antenna gain, and receiver antenna gain, respectively, and both G_{T} and G_{R} are 10 dB. The single-hop throughput is calculated by applying (10) and (13) and based on Figs. 17 and 20. Similarly, the multihop throughput is calculated by applying (11) and (13) and based on Table 8.

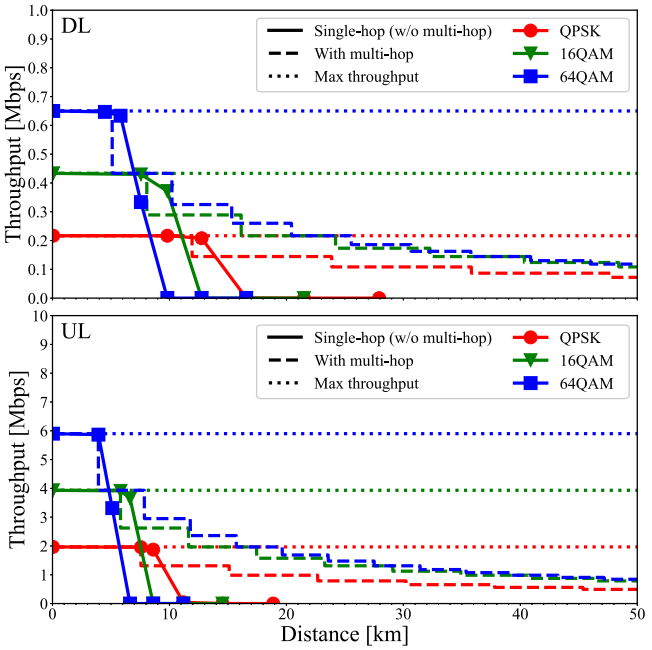

FIGURE 21. Transmission distance between RSs to throughput in typical urban model (DL:UL = 9:38).

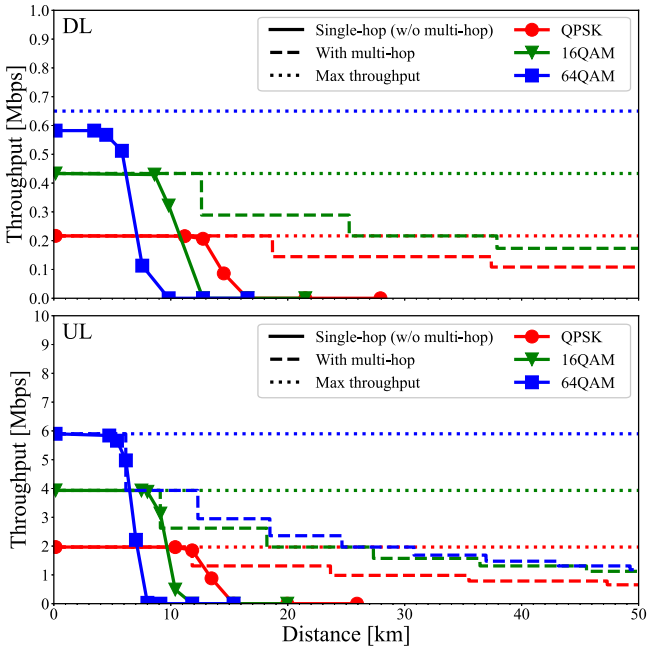

FIGURE 22. Transmission distance between RSs to throughput in profile A model with MRC diversity (DL:UL = 9:38).

Fig. 21 shows the transmission distance versus throughput in a typical GSM urban model. This result indicates that single-hop transmission was achieved up to approximately 9.0 km, even when QPSK was used. Conversely, when using

multihop transmission, although the transmission speed is approximately 1/2 to 1/6 (almost 1.0 Mbps for UL and 0.1 Mbps for DL), the maximum transmission distance is approximately 50 km. Because UL transmission has a throughput of 1.0 Mbps, 10,000 sensors with a throughput of 100 kbps can be accommodated. More sensors can also be accommodated by bundling multiple channels or by repeatedly using the same channel. It is also expected to be used in V2X based on the application. We set a large UL ratio primarily for collection purposes. Conversely, it is possible to change the DL:UL ratio based on the use cases.

Fig. 22 shows the transmission distance versus throughput with MRC diversity reception in the IEEE 802.22 profile A model. Under these conditions, the multihop relay is not evaluated because an error floor occurs in the DL-64QAM, and the input power required to achieve the required BER does not exist. In addition, the same tendency as the typical GSM urban model without MRC diversity was obtained for the transmission distance. The BS is expected to have higher antennas, particularly in a suburban environment.

VIII. CONCLUSION

In this article, we summarized the use cases and specifications of the ARIB T103/IEEE 802.16n system and comprehensively evaluated the transmission performance using the proposed methods in a VHF-band radio propagation environment through computer simulation and experimental evaluation by using the prototype. The experimental evaluation results confirmed the validity of computer simulations in this environment. Single-hop transmission reaches up to approximately 10 km while maintaining transmission speeds of several Mbps on the UL, when QPSK is used. Conversely, by using multihop transmission, although the transmission speed is approximately 1/2 to 1/6 (almost 1.0 Mbps for UL and 0.1 Mbps for DL), the maximum transmission distance is approximately 50 km. These results indicate that the ARIB T103/IEEE 802.16n is expected to be a WRAN communication system for IoT and V2X-based applications. In future studies, we aim to conduct transmission-characteristic experiments in outdoor environments using this prototype and determine the feasibility of achieving a communication distance of 10 km or more by using the ARIB T103/IEEE 802.16n-based WRAN.

REFERENCES

[1] K. Makino, K. Mizutani, T. Matsumura, and H. Harada, "A transceiver design of VHF band standardized broadband mobile communications systems," in *Proc. IEEE 20th Int. Symp. Wireless Pers. Multimedia Commun.*, 2017, pp. 87–93.

[2] J. Wu, S. Luo, S. Wang, and H. Wang, "NLES: A novel lifetime extension scheme– for safety-critical cyber-physical systems using SDN and NFV," *IEEE Internet Things J.*, vol. 6, no. 2, pp. 2463–2475, Apr. 2019.

[3] Y. Li, L. Yang, S. Han, X. Wang, and F.-Y. Wang, "When LPWAN meets ITS: Evaluation of low power wide area networks for V2X communications," in *Proc. 21st Int. Conf. Intell. Transp. Syst.*, 2018, pp. 473–478.

[4] S. Popli, R. K. Jha, and S. Jain, "A survey on energy efficient narrowband Internet of Things (NBIoT): Architecture, application and challenges," *IEEE Access*, vol. 7, pp. 16739–16776, 2019.

[5] G. Stanco, A. Botta, F. Frattini, U. Giordano, and G. Ventre, "On the performance of IoT LPWAN technologies: The case of Sigfox, LoRaWAN and NB-IoT," in *Proc. IEEE Int. Conf. Commun.*, 2022, pp. 2096–2101.

[6] D. Abada, A. Massaq, A. Boulouz, and M. B. Salah, "An adaptive vehicular relay and gateway selection scheme for connecting VANETs to internet via 4G LTE cellular network," in *Proc. IEEE Int. Conf. Comput. Sci. Renewable Energies*, 2019, pp. 1–8.

[7] *IEEE Standard for Information technology–Local and metropolitan area networks–Specific requirements–Part 11: Wireless LAN Medium Access Control (MAC) and Physical Layer (PHY) Specifications Amendment 6: Wireless Access in Vehicular Environments*, IEEE Standard 802.11pTM-2010, IEEE, NJ, USA, Jul. 2010.

[8] R. Atallah, M. Khabbaz, and C. Assi, "Multihop V2I communications: A feasibility study, modeling, and performance analysis," *IEEE Trans. Veh. Technol.*, vol. 66, no. 3, pp. 2801–2810, Mar. 2017.

[9] *IEEE Standard for Information technology–Local and metropolitan area networks–Specific requirements–Part 22: Cognitive Wireless RAN Medium Access Control (MAC) and Physical Layer (PHY) specifications: Policies and procedures for operation in the TV Bands*, IEEE Standard 802.22TM-2011, IEEE, NJ, USA, Jul. 2011.

[10] K. Hasegawa, M. Takekawa, K.-B. Toh, K. Yanagisawa, S. Sasaki, and M. Asano, "IEEE 802.22-based WRAN system for disaster-resistant network systems," in *Proc. IEEE Region 10 Humanitarian Technol. Conf.*, 2013, pp. 264–269.

[11] K. Ishizu et al., "Field experiment of long-distance broadband communications in TV white space using IEEE 802.22 and IEEE 802.11af," in *Proc. Int. Symp. Wireless Pers. Multimedia Commun.*, 2014, pp. 468–473.

[12] R. Ouyang, T. Matsumura, K. Mizutani, and H. Harada, "Software-defined radio-based evaluation platform for highly mobile IEEE 802.22 system," *IEEE Open J. Veh. Technol.*, vol. 3, pp. 167–177, 2022.

[13] *IEEE Standard for Local and metropolitan area networks Part 16: Air Interface for Broadband Wireless Access Systems*, IEEE Standard 802.16-2009, IEEE, NJ, USA, Mar. 2009.

[14] B. Li, Y. Qin, C. P. Low, and C. L. Gwee, "A survey on mobile WiMAX [wireless broadband access]," *IEEE Commun. Mag.*, vol. 45, no. 12, pp. 70–75, Dec. 2007.

[15] M. F. Mohamad, M. A. Saeed, and A. U. Priantoro, "Downlink channel estimation and tracking in mobile WiMAX systems," in *Proc. IEEE Int. Conf. Comput. Commun. Eng.*, 2008, pp. 1340–1343.

[16] S. Galih, R. Karlina, F. Nugroho, A. Irawan, T. Adiono, and A. Kurniawan, "High mobility data pilot based channel estimation for downlink OFDMA system based on IEEE 802.16e standard," in *Proc. IEEE Int. Conf. Elect. Eng. Inform.*, 2009, pp. 478–483.

[17] S.-L. Su, Y.-C. Lin, C.-C. Hsu, and G. C. H. Chuang, "A DFT-based channel estimation scheme for IEEE 802.16e OFDMA systems," in *Proc. IEEE 12th Int. Conf. Adv. Commun. Technol.*, 2010, pp. 775–779.

[18] *200 MHz-band broadband wireless communication systems between portable BS and MS*, ARIB STD-T103 Version 1.0, ARIB, Tokyo, Japan, Mar. 2011.

[19] M. Oodo and H. Harada, "Current status of 200 MHz-band public broadband wireless communication system," in *Proc. Int. Symp. Wireless Pers. Multimedia Commun.*, 2014, pp. 759–764.

[20] *IEEE Standard for Air Interface for Broadband Wireless Access Systems–Amendment 2: Higher Reliability Networks*, IEEE Standard 802.16n-2013, IEEE, NJ, USA, Mar. 2013.

[21] H. Harada, K. Makino, K. Mizutani, and T. Matsumura, "A TV white space wireless broadband prototype for wireless regional area network," in *Proc. 21st Int. Symp. Wireless Pers. Multimedia Commun.*, 2018, pp. 206–211.

[22] H. Harada, K. Mizutani, J. Fujiwara, K. Mochizuki, K. Obata, and R. Okumura, "IEEE 802.15.4g based Wi-SUN communication systems," *Inst. Electron.,Inf. Commun. Engineers Trans. Commun.*, vol. E100-B, no. 7, pp. 1032–1043, Jul. 2017.

[23] R. Molina-Masegosa and J. Gozalvez, "LTE-V for sidelink 5G V2X vehicular communications: A New 5G technology for short-range vehicle-to-everything communications," *IEEE Veh. Technol. Mag.*, vol. 12, no. 4, pp. 30–39, Dec. 2017.

[24] W. C. Jakes, "A comparison of specific space diversity techniques for reduction of fast fading in UHF mobile radio systems," *IEEE Trans. Veh. Technol.*, vol. 20, no. 4, pp. 81–92, Nov. 1971.
[25] H. Harada and R. Prasad, *Simulation and Software Radio for Mobile Communications*, Norwood, MA, USA: Artech House, 2002.
[26] J. Cho and Z. J. Haas, "On the throughput enhancement of the downstream channel in cellular radio networks through multi-hop relaying," *IEEE J. Sel. Areas Commun.*, vol. 22, no. 7, pp. 1206–1219, Sep. 2004.
[27] *Monte Carlo Simulation Methodology for the Use in Sharing and Compatibility Studies Between Different Radio Services or Systems*, Rep. ITU-R SM.2028, ITU-R, Geneva, Switzerland, Jan. 2001.

KIMINOBU MAKINO (Graduate Student Member, IEEE) received the B.E. degree in electric and electrical engineering and the M.I. degree in communications and computer engineering in 2015 and 2017, respectively, from Kyoto University, Kyoto, Japan, where he is currently working toward the Ph.D. degree with the Graduate School of Informatics and the School of Platforms. Since 2017, he has been a Researcher with the Science and Technology Research Laboratories, Japan broadcasting corporation (NHK), Tokyo, Japan. He researches WRAN systems in VHF band with Kyoto University and wireless links for mobile live programs at NHK. His research interests include ITS, multi-hop relay networks, machine learning, and MIMO technologies aiming for the B5G/6G.

KEIICHI MIZUTANI (Member, IEEE) received the B.E. degree in engineering from Osaka Prefecture University, Sakai, Japan, in 2007, and the M.E. and Ph.D. degree in engineering from the Tokyo Institute of Technology, Tokyo, Japan, in 2009 and 2012, respectively. He is currently an Associate Professor with the Graduate School of Informatics, Kyoto University, Kyoto, Japan. In 2010, he was an invited Researcher with Fraunhofer Heinrich Hertz Institute, Berlin, Germany. From 2012 to 2014, he was a Researcher with the National Institute of Information and Communications Technology. From 2014 to 2021, he was an Assistant Professor with the Graduate School of Informatics, Kyoto University. From 2021 to 2022, he was an Associate Professor with the School of Platforms, Kyoto University. His current research interests include physical layer technologies in white space communications, dynamic spectrum access, wireless smart utility networks, and 4G/5G/6G systems, including OFDM, OFDMA, MIMO, multi-hop relay network, and full-duplex cellular systems. Since joining in NICT, he has been involved in IEEE 802 standardization activities, namely 802.11af, 802.15.4m, and 802.22b. He was the recipient of the Special Technical Awards from IEICE SR technical committee in 2009 and 2017, Best Paper Award from IEICE SR technical committee in 2010 and 2020, Young Researcher's Award from IEICE SRW technical committee in 2016, Best Paper Award from WPMC2017 and WPMC2020, and Best Paper Presentation Award (1st Place) from IEEE WF-IoT 2020.

TAKESHI MATSUMURA (Member, IEEE) received the M.S. degree in electronic engineering and the Ph.D. degree in nano-mechanics engineering from Tohoku University, Sendai, Japan, in 1998 and 2010, respectively. From 1998 to 2007, he had been engaged in the Research and Development of wireless communications devices in some companies. In 2007, he joined the National Institute of Information and Communications Technology, Tokyo, Japan, as a Researcher with Smart Wireless Laboratory and engaged in the white-space communication systems and 5th generation mobile communication systems. From April 2016 to March 2019, he was an Associate Professor with the Graduate School of Informatics, Kyoto University, Kyoto, Japan. He is currently the Director of Wireless Systems Laboratory, NICT, and a Researcher with the Graduate School of Informatics, Kyoto University. His research interests include whitespace communication systems, wide-area wireless network systems, beyond 5G mobile communication systems, and wireless emulation technologies.

HIROSHI HARADA (Senior Member, IEEE) is currently a Professor with the Graduate School of Informatics, Kyoto University, Kyoto, Japan, and a Research Executive Director of the Wireless Networks Research Center, National Institute of Information and Communications Technology (NICT). In 1995, he joined the Communications Research Laboratory, Ministry of Posts and Communications (currently, NICT). From 2005 to 2014, he was a Visiting Professor with the University of Electro Communications, Tokyo, Japan. Since 1995, he has been researching on the topic of software defined radio, cognitive radio, dynamic spectrum access network, wireless smart ubiquitous network, and broadband wireless access systems on VHF, UHF, microwave, and millimeter-wave bands. In 2014, he was a Professor with Kyoto University. He has also joined many standardization committees and forums in U.S. and Japan and fulfilled important roles for them, especially IEEE 1900 and IEEE 802. He was the Chair of IEEE DySpan Standards Committee and Vice Chair of IEEE 802.15.4g, IEEE 802.15.4m, 1900.4, and TIA TR-51. He has authored the book entitled *Simulation and Software Radio for Mobile Communications* (Artech House, 2002). He was the Board of Directors of IEEE communication society standards board, SDR forum, DSA alliance, and whitespace alliance. He is a Co-Founder of Wi-SUN alliance and was the Chairman of the Board. He is currently the Vice Chair of IEEE 2857, IEEE 802.15.4aa, and Wi-SUN alliance. He was also the Chair of the IEICE Technical Committee on Software Radio and Public Broadband Mobile Communication Development Committee, ARIB. He is also involved in many other activities related to telecommunications. He was the recipient of the achievement awards in 2006 and 2018 and Fellow of IEICE in 2009, respectively, and achievement awards of ARIB in 2009, 2018, and 2022, respectively, on the topic of research and development on cognitive radio and wireless smart utility network.